Open Access

Journal of Energy and Power Technology

Original Research

Hierarchically-Structured Ti/TiO_2 Electrode for Hydrogen Evolution Synthesized via 3D Printing and Anodization

Xiang Li [1], Yuan Xue [2], Ryan Dehoff [3], Costas Tsouris [3], Patricia Taboada-Serrano [1, 4, *]

1. Microsystems Engineering PhD Program, Rochester Institute of Technology, 77 Lomb Memorial Drive, Rochester, NY, USA; E-Mails: lixiang980227@gmail.com; ptsche@rit.edu
2. Materials Science Program, University of Rochester, 4011 Wegmans Hall, PO Box 270166, Rochester, NY, USA; E-Mail: yxue83@gmail.com
3. Oak Ridge National Laboratory, 1 Bethel Valley Rd, Oak Ridge, TN, USA; E-Mails: dehoffrr@ornl.gov; tsourisc@ornl.gov
4. Chemical Engineering, Rochester Institute of Technology, 160 Lomb Memorial Drive, Rochester, NY, USA

* **Correspondence:** Patricia Taboada-Serrano; E-Mail: ptsche@rit.edu

Academic Editor: Alfonso Chinnici

Special Issue: Hydrogen Energy: Sustainable Production, Storage and Utilisation

Journal of Energy and Power Technology
2020, volume 2, issue 2
doi:10.21926/jept.2002007

Received: April 09, 2020
Accepted: May 08, 2020
Published: May 09, 2020

Abstract

Hierarchically-structured, electro-catalysts consisting of a titanium core with controlled macro-porosity and a thin titania surface-layer with controlled nano-porosity were synthesized via combination of additive manufacturing and in-situ anodization. The electrodes were tested for hydrogen evolution reaction and depicted competitive electro-catalytic activities, with Tafel slopes between 40 and 56 mV dec^{-1}. The electrodes also depicted competitive onset and over potentials when compared with other electrode alternatives. The synthesis approach for the electro-catalysts reported in this work is being extended to other metal/metal-oxide pairs and applications.

Keywords

3D printing; titanium dioxide nanotubes; anodization; water electrolysis; hydrogen evolution reaction

1. Introduction

One of the most attractive renewable-energy fuel alternatives is hydrogen. Hydrogen is an ideal chemical energy carrier with energy density of 140 MJ kg^{-1} and no secondary contaminants generated during its oxidation [1]. Currently, hydrogen is mainly obtained from natural gas and coal, involving consumption of fossil fuels along with greenhouse gas release [2]. Securing a clean, safe, and sustainable approach for renewable hydrogen production has become one of the biggest barriers that hinder the leap from fossil-fuel-based energy society to hydrogen energy economy.

Water is naturally the most promising source for hydrogen production due to its abundance, low cost, and easy access on earth. Consequently, a great deal of effort has been devoted to generating hydrogen from water through sustainable, energy-efficient, and cost-effective processes that have the potential to work at industrial scales, such as photocatalytic water splitting and electrolysis [3-6]. The hydrogen evolution reaction (HER), $2H^+ + 2\bar{e} \rightarrow H_2$, is the basis for water splitting-based hydrogen production. In order to reach high energy-efficiency, catalysts are widely used to minimize the potential required to initiate the HER [7]. The best-known catalysts for the HER to date are noble metals, such as platinum. However, the scarcity and high price of noble metals substantially limit their large-scale deployment [8].

Developing precious-metal-free catalysts for HER is a crucial step in moving towards a hydrogen-based energy economy. Molybdenum sulfide materials are one of the typical non-noble metal catalysts explored as alternative to platinum-group catalysts due to their high electro-catalytic activity and stability for HER [9-11]. The synthesis of molybdenum-based catalysts, however, usually involves energy-intensive, time-consuming, and complex processes that might hinder their application at industrial scales. For example, ultra-vacuum processing [10], high-temperature treatment [12], and sulfidization under H_2S gas are some of the steps involved in the molybdenum-based-catalysts synthesis [10].

In 1972, Honda and Fujishima reported the occurrence of photocatalytic water-splitting by using crystalline titanium dioxide (TiO_2) electrode for hydrogen production. This opened the door for producing hydrogen from solar energy through a clean, low-cost, and environmentally friendly approach [13]. The finding reported by Honda and Fujishima triggered thousands of publications dealing with exploring TiO_2 photocatalytic activity for hydrogen production [14-19]. It is not surprising that TiO_2 has become one of the most common catalysts for photocatalytic hydrogen production owing to its abundance, low cost, and semiconductor properties. However, the wide band gap (3.2 ēV) limits the photocatalytic activity of TiO_2 to UV light only [20]. Therefore, the past decade has witnessed the proliferation of a wide range of studies geared towards improving the visible light absorption of TiO_2 via doping of TiO_2 with metal ions [21], coupling TiO_2 with low band gap semiconductor materials [22, 23], dye sensitization of TiO_2 [19], surface modification of TiO_2 [24], and also the use of TiO_2 as support for noble metals [25, 26]. Enormous efforts have been devoted to the enhancement of TiO_2 photocatalytic activity via increasingly complex chemical functionalization. For example, Ag_2S-coupled TiO_2 nanowire fabrication requires hydrothermal

treatment over 72 hours [22], and cobalt-oxide loaded TiO_2/CdS composites synthesis consists of 12-hours reaction under vigorous stirring and drying under vacuum at 333 K for another 12 hours. While photocatalytic activity has significantly improved through these methods, the potential for application of these catalysts at industrial scales is lowered by their increased complexity [18].

Another methodology explored for improving the performance of TiO_2-based catalysts for photocatalytic hydrogen generation is to control catalyst architecture as a means to improve catalyst activity. Employing a core-shell structure is an efficient strategy in order to control architecture. Yang et al. [27-29] reported a good photocatalytic activity with a hydrogen production rate of 0.258 mmol h^{-1} g^{-1} for a core-shell nanostructure of rutile TiO_2 with sulfide surface (TiO_2-x:S). Kim and co-workers [28] developed a core/shell structure of magnetic nanoparticles $NiFe_2O_4$/TiO_2 and successfully applied it to photo-driven HER. Although core-shell structures show good catalytic performance for HER, a concern with core/shell designs is the poor contact between the core and shell materials [30]. It usually results in a dramatic decrease of catalytic activity with continuous use.

Embracing three-dimensional (3D) geometry for electrodes has become evident as another attractive way of obtaining high performing HER photo-catalysts. For instance, Xu et al. utilized a multiscale 3D TiO_2 platform decorated with graphene quantum dots for photo-electro-chemical hydrogen production. Li et al. [31] developed a 3D Pt/TiO_2 architecture via a solvo-thermal method. The 3D Pt/TiO_2 electrode exhibited high photocatalytic activity during hydrogen production tests [31]. However, a noble metal is still required to boost the photocatalytic activity of TiO_2 [32].

All the efforts detailed above were focused on improving photo-catalytic activity of TiO_2 for hydrogen production. To our knowledge, only the inclusion of TiO_2 nanoparticles on other metal catalysts has been explored for electro-catalytic HER in the absence of light; and the presence of TiO_2 has been identified as contributing to improved electrocatalytic activity for HER [33, 34].

Recently, 3D printing has been introduced as the means to manufacture micro-reactors and reactor components [35]. This new approach to the manufacture of reactor components is driven by the goal of process intensification, and can certainly be incorporated into the manufacture of catalysts as well. In this work, we report on the performance of a hierarchically structured Ti-core/TiO_2-coating electro-catalyst for HER in the absence of light (no photo-catalysis involved). The electro-catalysts were produced via 3D printing and in-situ anodization, in order to superimpose highly-ordered TiO_2 nanotubes (NTs) onto hierarchically 3D Ti-metal templates used as current collectors. The reported hierarchically structured Ti/TiO_2 materials were tested in this study for HER electro-catalytic activity, and were found to be good candidates to overcome the hurdles towards renewable, industrial-scale hydrogen production. To our knowledge, this work presents the first utilization of titanium and titania for electro-catalytic HER in the absence of light. A similar synthesis approach to the one reported in this work is being pursued and can be used for other metal/metal oxide combinations, not reported in the present work.

2. Materials and Methods

2.1 Synthesis of the Hierarchical Flow-Through 3D Ti/TiO_2 NT Electrode

Macro-porous, flow-through 3D Ti templates were printed with an additive manufacturing method using ARCAM Electron Beam Melting equipment [36, 37]. The templates had dimensions of 2.5 × 2.5 × 0.22 cm. Titanium dioxide nanotube (TiO_2 NT) arrays were grown on the surface of

the 3D Ti templates via anodization following the methodologies described in previous work [38-41]. Two formulation of anodization baths were used to grow the TiO_2 NT layer on different 3D Ti templates: (a) an organic-solvent-based anodization solution (EG-anodization solution), and (b) an aqueous-solvent-based anodization solution (W-anodization solution). The preparation of samples and anodization solutions are described below, along with the anodization conditions in each case.

In all cases, the 3D Ti templates were thoroughly rinsed with ethanol and air-dried prior to the anodization procedures. The EG-anodization solution was prepared by mixing 147 mL ethylene glycol, 3 mL of distilled water, and 280 mg of ammonium fluoride. The EG-anodization solution was introduced into a temperature-controlled anodization cell under dry air. The anodization system consists of (a) a Princeton Applied Research K0235 flat cell with a platinum mesh counter electrode, (b) a TDK-Lambda ZUP 1203.6/U power supply, and (c) an Agilent Technologies Digital Multimeter 5 1/2-Digit Display. These three instruments are connected to a computer and controlled by a custom-developed LabVIEW code, as depicted in Figure 1. The sample was anodized at 15 °C for 1 hour in this solution with a platinum counter-electrode at a fixed voltage of 60V. After anodization, the electrode was removed from solution, rinsed with methanol, and allowed to air-dry. Electrodes synthesized in the EG-anodization solutions will be referred to as ***Ti/TiO$_2$-NT-EG*** in this work.

The W-anodization solution was prepared by mixing 300 mL DI water and 576.2 mg ammonium fluoride. The pH value of the W-anodization solution was increased to 3.0 by adding drops of sulfuric acid. The anodization process with W-anodization solution was carried out at 15 °C for 1 hour with a platinum counter-electrode at fixed voltages of 20V in the temperature-controlled anodization cell under dry air depicted in Figure 1. After anodization, the electrode was removed from solution, rinsed with methanol, and allowed to air-dry. Electrodes synthesized in the W-anodization solutions will be referred to as ***Ti/TiO$_2$-NT-W*** in this work.

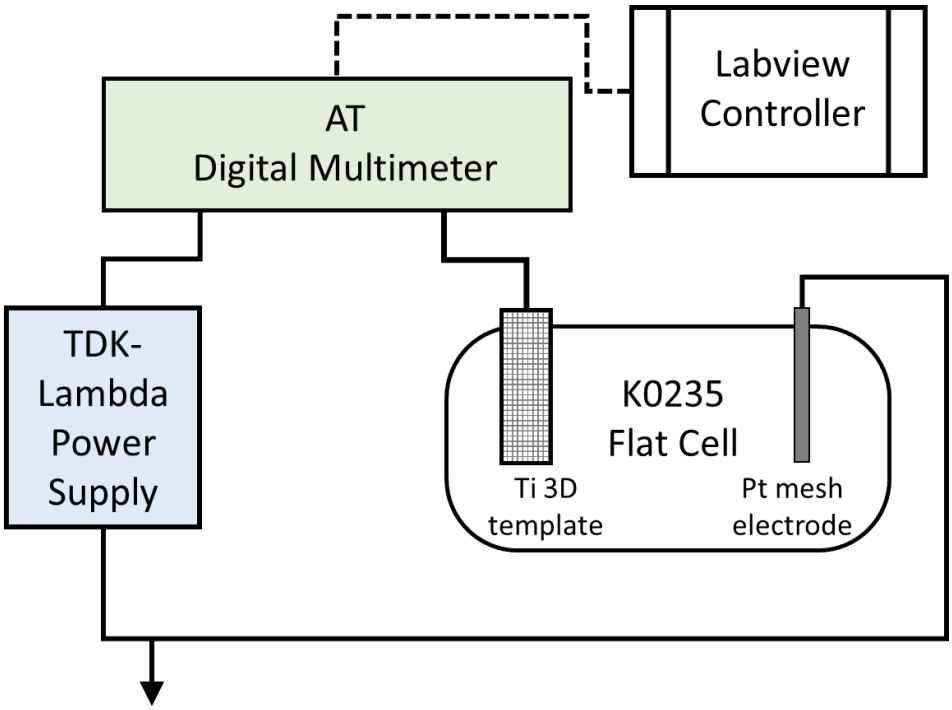

Figure 1 Schematic of the custom-built anodization system used for anodization of the 3D Ti templates.

The morphology of the hierarchical flow-through Ti/TiO_2 electrode was examined by scanning electron microscopy equipped with electron dispersive spectroscopy (SEM-EDS). SEM images and EDS spectra were obtained using the MIRA3 field emission SEM (TESCAN, PA) equipped with Bruker x-flash energy-dispersion microanalysis system (Bruker, MA). Imaging was used to examine the geometry of the TiO_2 NTs for all samples and for measuring diameters, lengths, and density of packing, following the procedure to calculate specific surface area described in previous work [38, 39]. Measurements of BET specific surface area were also performed, but were used only as reference since the relatively large weight of the samples added uncertainty to the results.

Finally, X-ray diffraction measurements (XRD) on the samples were also attempted, but the intricate geometry hindered the resolution of the results.

2.2 Hydrogen Evolution Reaction Testing

The electrochemical measurements were performed at room temperature using a BASi Cell stand controlled by a BASi C3 potentiostat, in which the working electrodes were the different 3D Ti/TiO_2 electrodes prepared as detailed above, the counter electrode was a BASi MW-1032 platinum electrode, and the reference electrode was BASi Ag/AgCl (BASi MW-2052). All potentials reported in this work were normalized to that of the reference hydrogen electrode (RHE). Polarization curves were obtained by linear sweep voltammetry (LSV) test, which is carried out by sweeping the potential from -0.35 V to 0.05 V with a sweep rate of 5 mV s^{-1} at room temperature in 0.5 M H_2SO_4. Preliminary tests on the stability of the electrodes were performed by monitoring current during HER in a 0.5 M H_2SO_4 solution during 10 hours of operation at a constant applied potential of -150 mV and at a temperature of 25 °C. Electrochemical impedance spectroscopy (EIS) tests were performed in the same configuration at an over-potential of 500 mV with frequency ranging from 1 MHz to 1 kHz by Gamry Reference 6000 (Gamry, PA).

No human, animal, plant, or subjects were involved in the study.

3. Results

3.1 Characterization of the 3D Ti/TiO_2 Electrodes

Figure 2 presents images of the morphology of one of the ***3D Ti/TiO_2-NT-EG*** electrodes at increasing degrees of magnification: a photographic image (Figure 2a) and several images obtained by scanning SEM (Figure 2b-f). Figure 1a is the image of 3D Ti/TiO_2 NT electrode after anodization. The 3D Ti/TiO_2 NT electrode has visible hierarchical structure, with macro-porosity and micro-porosity (nanopores). The macro-porosity provides unique flow-through features, which maximize the contact area between the electrolyte and active catalyst surface (TiO_2 NT). From Figure 2b, one can observe that the grid of 3D templates is about 1-mm and the grid-layer distance is about 0.5 mm. These features can be adjusted by modifying the 3D printing parameters. Assisted by the 3D printing technique, the 3D electrode framework can be easily produced for large-scale operations via a reliably reproducible approach. The TiO_2 NT layer grafted onto the surface of 3D Ti templates via *in situ* anodization can be clearly visualized in Figures 2c and 2d. The 3D Ti templates are completely wrapped by the TiO_2 NT layers. Minor charging (bright areas) is also observed due to the conductivity difference between the Ti template and the TiO_2 NT layer. Figures 2e and 2f clearly depict the nanotube structure of the TiO_2 NT layer.

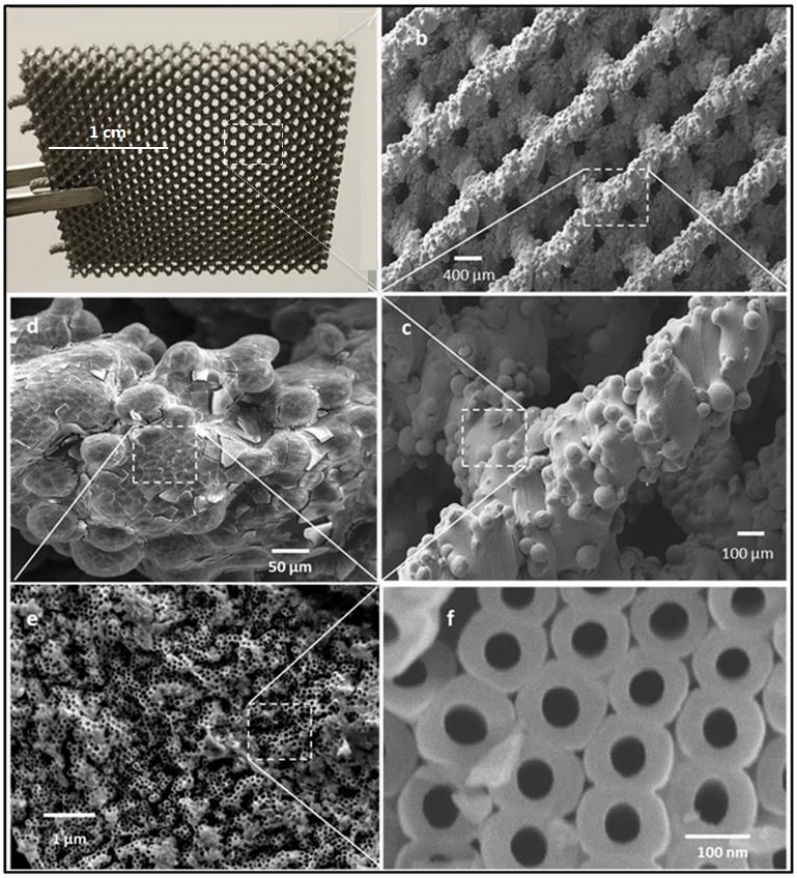

Figure 2 Image and SEM micrographs of 3D Ti/TiO_2-NT-EG under various degrees of magnification.

Figure 3 depicts SEM images of identical 3D Ti templates anodized with the two solutions described in this work, the W-anodization and the EG-anodization solutions. The TiO_2 NT synthesized with the two different formulations of anodization solutions on identical 3D Ti templates showed significant variation in morphology at the nano-scale. By comparing Figures 2a and 2b, it is apparent that the morphological structures of ethylene-glycol-based TiO_2 NT (***TiO_2-NT-EG***) and water-based TiO_2 NT (***TiO_2-NT-W***) present differences in uniformity of tubular structure, cylindrical characteristics, and thickness of the nanotube walls. The ***TiO_2-NT-EG*** electrodes are uniform and have very distinct cylindrical shapes when compared to the ***TiO_2-NT-W*** electrodes. Furthermore, examination of Figures 2f, 3a, and 3b clearly shows that ***TiO_2-NT-EG*** electrodes have thicker walls.

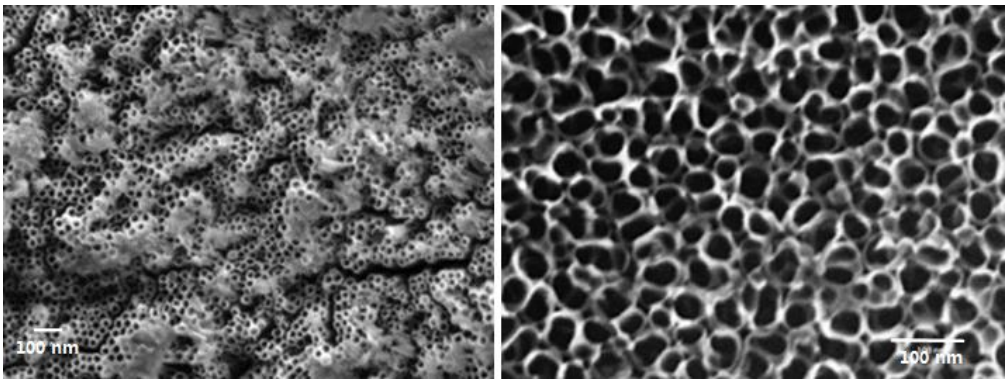

Figure 3 Morphology of (a) ***3D Ti/TiO_2-NT-EG***, and (b) ***3D Ti/TiO_2-NT-W***.

Energy dispersive X-ray spectroscopy (EDS) results confirmed the successful anodization of TiO_2 NT on the surface of 3D Ti template (Figure 4) with the two electrolyte-formulations used in this work (i.e., ethylene glycol-based and water-based anodization solutions). Figure 4a depicts the EDS pattern of the bare 3D Ti templates, in which an oxygen peak cannot be found. Electrodes fabricated via anodization with the two anodization solutions clearly present oxygen peaks around 0.5 KēV in Figures 4b and 4c, corresponding to the ***TiO_2-NT-EG*** and ***TiO_2-NT-W***, respectively. This confirms that the nanotube structure observed via SEM on the surface of 3D Ti templates is made of TiO_2. It is worth pointing out that the intensity of oxygen peak for ***TiO_2-NT-EG*** is slightly larger than that of ***TiO_2-NT-W***. This fact substantiates the observations via SEM that water-based anodization formulations result in thin-walled, densely packed TiO_2 nanotubes with a smaller amount of oxide material present. Furthermore, the specific surface area for the ***3D TiO_2-NT-EG*** samples was equal to 0.88 m^2/g, while the specific surface area of the ***3D TiO_2-NT-W*** samples was equal to 1.48 m^2/g. These areas, determined via the statistical procedure described in previous work and corroborated via BET measurements, seem very low from the usual values expected for catalysts. These numbers reflect the fact that 3D Ti templates are relatively heavy. Finally, the aluminum and carbon elements found in the 3D Ti/TiO_2-NT electrodes are necessary ingredients for the 3D-printing Ti ink.

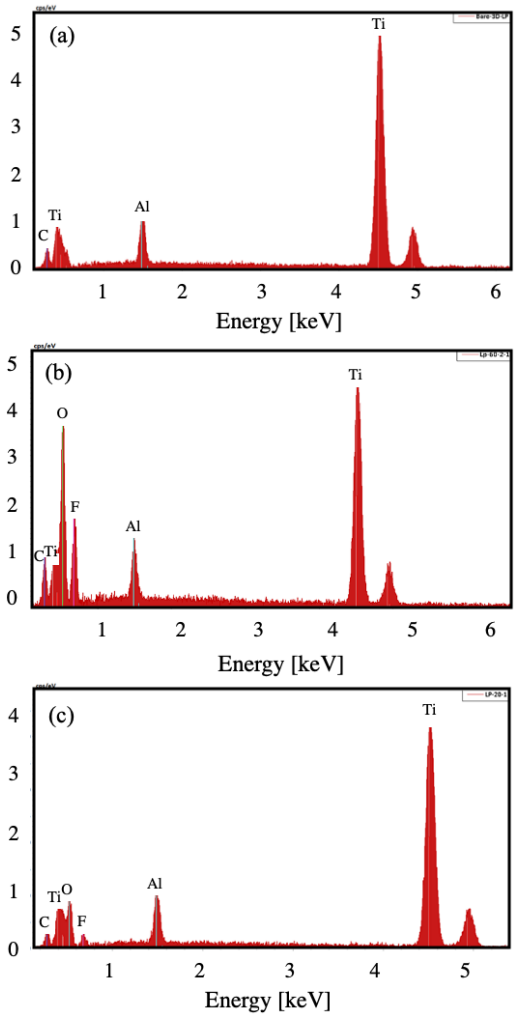

Figure 4 EDS spectra of (a) bare 3D Ti templates, (b) ***3D Ti/TiO_2-NT-EG***, and (c) ***3D Ti/TiO_2-NT-W***. The y-axis has units of cos/eV.

3.2 Hydrogen Evolution Reaction (HER) Activity

Upon successful synthesis of the 3D Ti/TiO_2 NT electrodes, their catalytic activity towards HER was carefully examined in a three-electrode test system with acid media. Figure 5 depicts the electro-catalytic performance of bare 3D Ti templates, ***3D Ti/TiO$_2$-NT-EG***, and ***3D Ti/TiO$_2$-NT-W*** for HER in a 0.5 M H_2SO_4 electrolyte. Figure 5a compares the polarization curves obtained via repetitive measurements for various electrode samples. The featureless polarization curve of bare 3D Ti templates demonstrates that the 3D Ti templates do not depict catalytic activity for HER, as expected due to the position of Ti on the reactive volcano plot for HER [42]. In contrast, both ***3D Ti/TiO$_2$-NT-EG*** and ***3D Ti/TiO$_2$-NT-W*** show high electrocatalytic activity during the tests, evidencing a sharp increase in catalytic reduction current density (Figure 4a). The onset potential of HER was measured as -45 mV vs RHE for ***3D Ti/TiO$_2$-NT-W*** and -87 mV vs RHE for ***3D Ti/TiO$_2$-NT-EG***, suggesting both types of hierarchical catalysts have good catalytic activity for HER. The dependence of over-potential (η) on the logarithmic current density (j) is depicted in Figure 5b. The linear relationships of η and log (j) observed in Figure 5b, namely the Tafel slope, can be used to hypothesize about the HER mechanism taking place in the hierarchical catalysts. Tafel slopes provide an indication of the possible mechanisms that may be taking place during an electrochemical reaction. Tafel slope values of 40 and 56 mV dec^{-1} were obtained for ***3D Ti/TiO$_2$-NT-W*** and ***3D Ti/TiO$_2$-NT-EG*** respectively, via linear regression of the above mentioned curves. When these values are compared with the Tafel slope of the state-of-the-art Pt/C catalyst (~ 30 mV dec^{-1}), one can suggest that the hierarchical electrodes studied in this work exhibit slightly lower HER catalytic activities than the commercial electrode, but not significantly lower.

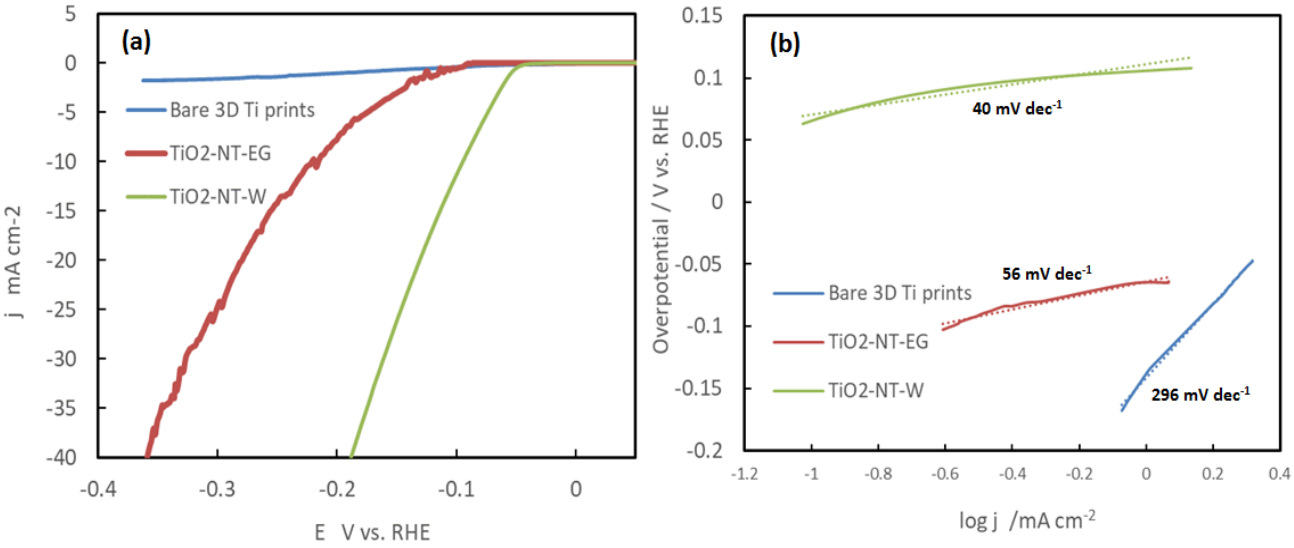

Figure 5 (a) Polarization curves for HER on bare 3D Ti templates, ***3D Ti/TiO$_2$-NT-EG***, and ***3D Ti/TiO$_2$-NT-W*** in 0.5 M H_2SO_4. (b) Tafel plots for the various samples derived from (a) obtained via linear regression shown in dotted lines.

Figure 6 compares the Tafel slopes obtained for the electro-catalysts reported in this work. The average Tafel slope obtained for the ***3D Ti/TiO$_2$-NT-W*** electrodes is smaller than that of other HER catalysts reported in recent literature (Figure 6), indicating that the ***3D Ti/TiO$_2$-NT-W*** catalyst is a promising candidate for industrial application.

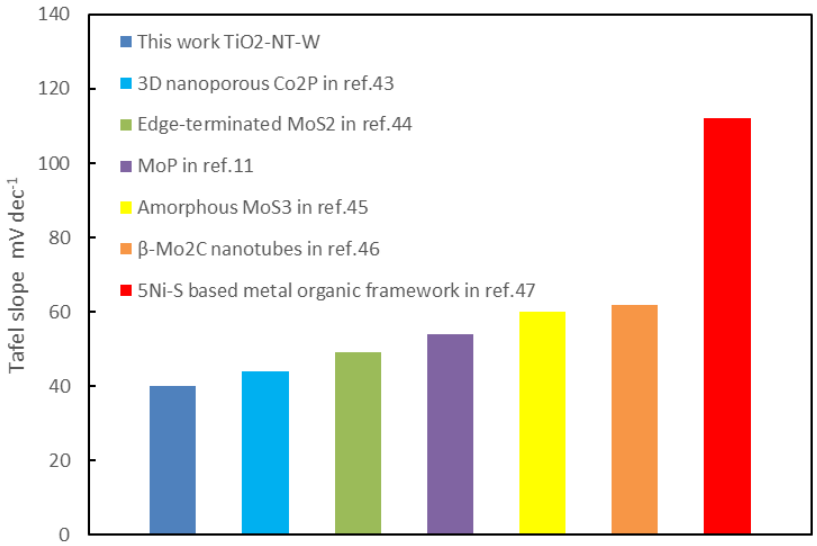

Figure 6 Comparison of Tafel slopes of various HER catalysts in recently published articles.

The onset potential for HER and the over-potential at a current density of 10 mA cm^{-2} measured for our electro-catalysts are compared with other promising catalysts reported in the literature for HER in Table 1. The average onset potential of the ***3D TiO_2-NT-W*** catalysts is -45 mV, which confirms that this catalyst is capable of triggering HER with energy requirements close to the commercial Pt/C catalyst. In order to reach 10 mA cm^{-2} current density, the average operation over-potential for the ***3D TiO_2-NT-W*** and the ***3D TiO_2-NT-EG*** electrodes are 92 and 215 mV, respectively. The exchange current density (j_0) for the ***3D TiO_2-NT-EG*** was determined to be equal to 7.68 × 10^{-3} mA cm^{-2}; and the value corresponding to ***3D TiO_2-NT-W*** was 2.13 × 10^{-4} mA cm^{-2}, from extrapolation of the Tafel plots. The electrochemical tests for HER performed in this work show that the ***3D Ti/TiO_2 NT-W*** electro-catalysts are competitive with recently documented HER catalysts, and that the catalytic activity of the ***3D Ti/TiO2-NT-EG*** electro-catalysts is not as high as that of the ***3D Ti/TiO_2-NT-W*** catalysts. In terms of the stability of both electrocatalysts, preliminary tests show a slight decrease of less than 5% of current density during the first hour of operation, and stabilization of the current at this level during the rest of the period of continuous operation per the test described in the methods section.

Table 1 Onset potential for HER and over-potential at 10 mA cm^{-2} for various catalysts.

Catalysts	**Onset potential (mV)**	**Over-potential (mV) at 10 mA cm^{-2}**
3D Ti/TiO_2-NT-W in this work	-45	92
3D Ti/TiO_2-NT-EG in this work	-87	215
3D nanoporous Co_2P [43]	-24	80
Edge-terminated MoS_2 [44]	-100	149
MoP [11]	-50	500
Amorphous MoS_3 [45]	-150	200
β-Mo_2C nanotubes [46]	-82	172
Ni-S based metal organic framework [47]	N/A	238

Electrochemical impedance spectroscopy (EIS) was employed to provide further insight into the electrode/electrolyte interface and the electrochemistry at the electrode surface. Figure 6 presents the Nyquist plots of representative EIS spectra obtained for both, ***3D TiO_2-NT-EG*** and ***3D TiO_2-NT-W*** electrodes, at 500 mV. The inset in Figure 7 depicts the electrical equivalent circuit (EEC) used to analyse the EIS spectra. The EEC consists of Ohmic resistance (R_s) in series with a module, in which the charge transfer resistance (R_{ct}) is in parallel with a constant phase element (CPE). The ***3D TiO_2-NT-W*** electrode exhibits R_{ct} with the value of 9.8 Ω, which is smaller than that corresponding to ***3D TiO_2-NT-EG*** with the value of 31.4 Ω. The high electron transfer rate on the ***3D Ti/TiO_2-NT-W*** electrodes is particularly noteworthy.

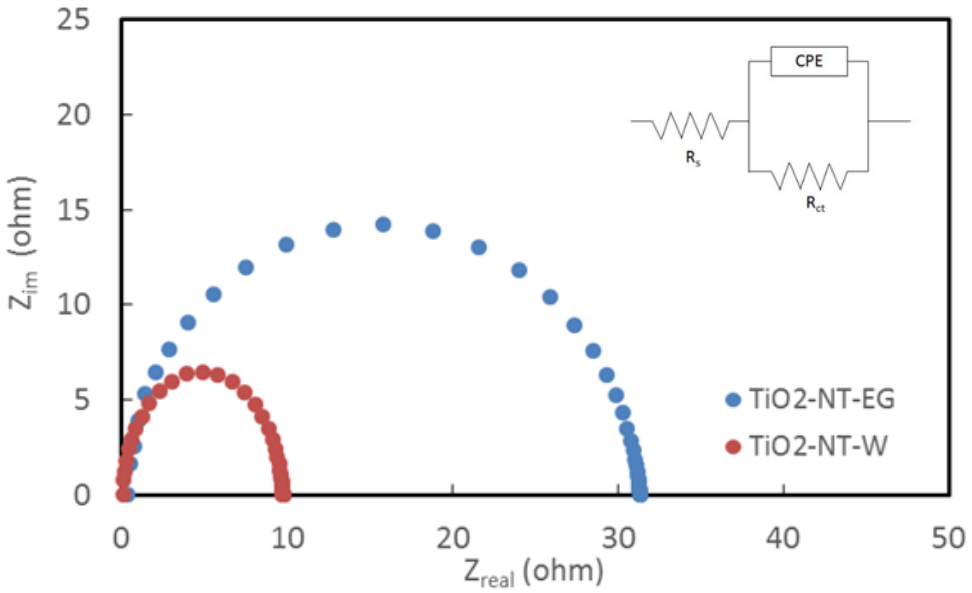

Figure 7 EIS Nyquist plots of ***3D Ti/TiO_2-NT-EG*** and ***3D Ti/TiO_2-NT-W***. Inset shows the electrical equivalent circuit used to explain the EIS spectra.

4. Discussion

The morphological differences between ***3D TiO_2-NT-EG*** and ***3D TiO_2-NT-W*** electrodes can be explained by the competitive effects taking place during TiO_2 NT growth. Two competitive reactions, oxidation (oxide-layer formation) and dissolution (etching) of the oxide layer, take place during the anodization process used to grow the TiO_2 NT layer on the 3D templates. Oxidation rates, and therefore mass of TiO_2 grown on 3D Ti templates, are highly dependent on the conductivity of the anodization bath and the Ohmic resistance at the surface of the electrode. Limited charge transfer during the anodization process is observed due to low electrical conductivity of the ethylene-glycol-based anodization bath, i.e., a larger resistive current drop. As a result, the mass of TiO_2 on the ***3D TiO_2 NT-W*** electrodes obtained during the same anodization time on the same 3D Ti templates was 38% of that obtained for the ***3D TiO_2-NT-EG*** electrodes. The differences in diameter, length, and wall thickness of the TiO_2 NTs among the electrodes stem from the fact that the water-based anodization solution promotes a higher chemical etching rate for the oxides (namely, TiO_2 NT), than the organic-based solution (ethylene glycol in the present study). The balance between the rates of oxide-layer formation and re-dissolution is offset towards re-dissolution of the oxide layer, resulting in thin-walled, shorter nanotubes in the

aqueous case. At the same time, TiO_2 NTs are longer, of smaller diameters and thicker walls in the case of ***3D TiO_2-NT-W*** electrodes. The morphological differences impact the electro-catalytic activity towards HER of both types of electrodes mainly due to the following factors: (a) the specific surface area is larger for the ***3D TiO_2-NT-W*** electrodes, i.e., larger catalytic surface; and (b) the semi-conductor layer (TiO_2 layer) is thinner for these electrodes as well, which translates into lower resistance.

The classical HER reaction mechanisms proposed for acid media (i.e., Volmer reaction, Heyrovsky reaction, and Tafel reaction) can be used as a framework to interpret the different values of Tafel slope for the 3D Ti/TiO_2-NT electrodes with HER kinetics [42, 46-49]. Specifically, in acidic and aqueous electrolyte, HER is usually comprised of three steps: (i) hydrogen adsorption (Volmer reaction); and (ii) reaction between adsorbed H and H^+ in solution to form free H_2 (Heyrovsky reaction); or (iii) reaction between two adsorbed H to form free H_2 (Tafel reaction). These steps are presented in equations (1) – (3), where M represents an active site.

$$\textit{Volmer step}: H_3O^+ + \bar{e} + M \leftrightarrow M\text{-}H + H_2O \quad (1)$$

$$\textit{Heyrovsky step}: M\text{-}H + H_3O^+ + \bar{e} \leftrightarrow H_2 + H_2O + M \quad (2)$$

$$\textit{Tafel step}: 2\,M\text{-}H \leftrightarrow H_2 + 2\,M \quad (3)$$

Extensive work by Conway and others has identified the adsorption of H^+ (Volmer reaction) as the critical mechanistic step leading to hydrogen formation [42]. Titanium (Ti), nickel (Ni), iron (Fe), and other metals are believed to exhibit poor electro-catalytic activity for HER due to their inability to readily adsorb H at low potentials [42, 50, 51]. Studies on single-crystal TiO_2, however, have demonstrated that TiO_2 can readily adsorb inorganic ions and molecules [50]. Tafel slopes obtained for single-crystal Pt vary between 40 mV dec^{-1} and 120 mV dec^{-1}, depending on the crystalline structure [47, 48]. Theoretically, values of Tafel slopes for HER are as follows: (a) 120 mV dec^{-1} for Volmer-reaction as rate-controlling step (H-adsorption is rate-limiting); (b) 40 to 120 mV dec^{-1} for Heyrovsky-reaction as rate-controlling step (reaction between adsorbed H and free H^+ is rate limiting); and (c) 30 mV dec^{-1} for Tafel-reaction as rate-controlling step (reaction between two adsorbed-H is rate limiting). HER on Pt is usually considered to occur via a Volmer-Heyrovsky mechanism, with the Heyrovsky step limiting the overall rate of reaction. The values of Tafel slopes measured for the ***3D Ti/TiO_2-NT-W*** electrodes (40 mV dec^{-1}) and the ***3D Ti/TiO_2-NT-EG*** electrodes (56 mV dec^{-1}) electrodes suggest that these electrodes may promote a Volmer-Heyrovsky mechanism.

Since it has been well documented that Ti displays no significant catalytic activity for HER [42, 52], the competitive catalytic activities towards HER presented by the electrodes in this work can be mainly attributed to the TiO_2 NT. The 3D Ti templates contribute as effective support and current collector for the active sites due to their high conductivity and very good electrical contact with the active surface itself. In previous studies, we used highly-ordered, cylindrical TiO_2 NTs on planar Ti templates to study the formation of electrical double layer (EDL) [38, 39]. Furthermore, those studies showed that electro-sorption of ions, and ion-size-exclusion effects, can be enhanced via tuning NT morphology, i.e., NT diameter, density, and length [38]. The crystalline structure of TiO_2 NTs (amorphous or anatase) can be easily tuned without changing morphology via annealing after synthesis, further enhancing electrical conductivity or even photo-catalytic-activity [38, 39]. Given the fact that the TiO_2 NT properties are associated with improved HER

reaction rates in this work, the combination of highly tailorable TiO_2 NT active surfaces with easily constructed 3D templates opens a door for a straight-forward method to engineer novel HER catalysts.

5. Conclusions

Summarizing, a novel strategy to fabricate hierarchically, flow-through 3D Ti/TiO_2-NT electrodes for HER was presented in this work. The 3D Ti/TiO_2-NT electrodes reported in the present work take advantage of 3D printing and in-situ anodization to achieve efficient HER electro-catalysis. Competitive catalytic activity for HER of our 3D Ti/TiO_2-NT electrodes can be ascribed to the following reasons: 1) the hierarchically flow-through 3D structure enables efficient utilization of the active catalytic surface (TiO_2 NT); 2) the TiO_2 NT structure on the 3D Ti/TiO_2-NT electrodes may trigger a Volmer-Heyrovski mechanism for HER at comparable onset potentials when compared to other emerging catalysts; and 3) the ohmic-free contact between catalyst (TiO_2 NT) and the current collector (3D Ti template) provides a continuous and efficient conducting network of charge and electron transfer. Further improvements in catalytic HER activity and performance of the present electrodes can easily be pursued via simple engineering of the highly ordered and tailorable structure and morphology of TiO_2 NTs. Finally, a clear advantage of the electrodes introduced in this work is that they are inexpensive and readily scalable for industrial applications, due to their straight-forward fabrication method. In addition, the 3D catalyst fabrication approach can be employed for a variety of metals including nickel, zirconium, and aluminum among others, as well as mixtures of metals.

Acknowledgments

The authors would like to acknowledge the following individuals and institutions:

- Richard Mayes of the Oak Ridge National Laboratory
- Richard Hailstone from the Chester F. Carlson Center for Imaging Science at Rochester Institute of Technology
- Brian McIntyre from the Institute of Optics at the University of Rochester
- Kate Gleason College of Engineering at the Rochester Institute of Technology

Author Contributions

Xiang Li performed the experimental work, analysis of data and contributed significantly to the preparation of the manuscript. Yuan Xue assisted with the EIS experiments and analysis of that set of data. Ryan Dehoff printed the 3D templates used in this work. Costas Tsouris assisted with the analysis of data, preparation, and revision of the manuscript. Patricia Taboada-Serrano supervised the work, analysed the data, and prepared and revised the manuscript.

Funding

Funding for this work was provided by the Laboratory Directed Research and Development Fund of the Oak Ridge National Laboratory and the Kate Gleason Fund.

This manuscript has been co-authored by UT-Battelle, LLC under Contract No. DE-AC05-00OR22725 with the US Department of Energy. The United States Government retains and the

Competing Interests

The authors have declared that no competing interests exist.

References

1. Wang M, Chen L, Sun L. Recent progress in electrochemical hydrogen production with earth-abundant metal complexes as catalyts. Energ Environ Sci. 2012; 5: 6763-6778.
2. Turner JA. Sustainable hydrogen production. Science. 2004; 305: 972-974.
3. Akhmal Saadon S, Sathishkumar P, Mohd Yusoff AR, Hakim Wirzal MD, Rahmalan MT, Nur H. Photocatalytic activity and reusability of ZnO layer syntehsized by electrolysis, hydrogen peroxide and heat treatment, Environ Technol. 2016; 37: 1875-1882.
4. Yu X, Prévot MS, Guijarro N, Sivula K. Self-assembled 2DWSe$_2$ thin films for photoelectrochemical hydrogen production. Nat Commun. 2015; 6: 7596.
5. Pop LC, Sygellou L, Dracopoulos V, Andrikopoulos KS, Sfaelou S, Lianos P. One-step electrodeposition of CdSe on nanoparticulate titania films and their use as sensitized photocanodes for photoelectrochemical hydrogen production. Catal Today. 2015; 252: 157-161.
6. Lin MY, Hourng LW. Effects of magnetic field and pulse potential on hydrogen production via water electrolysis. Int J Energy Res. 2014; 38: 106-116.
7. Walter MG, Warren EL, McKone JR, Boettcher SW, Mi Q, Santori EA, et al. Solar water splitting cells. Chem Rev. 2010; 110: 6446-6473.
8. Subbaraman R, Tripkovic D, Strmcnik D, Chang KC, Uchimura M, Paulikas AP, et al. Enhancing hydrogen evolution activity in water splitting by tailoring Li^+-Ni(OH)$_2$-Pt interfaces. Science. 2011; 334: 1256-1260.
9. Hinnemann B, Moses PG, Bonde J, Jørgensen KP, Nielsen JH, Horch S, et al. Biomimetic hydrogen evolution: MoS$_2$ nanoparticles as catalysts for hydrogen evolution. J Am Chem Soc. 2005; 127: 5308-5309.
10. Jaramillo TF, Jørgensen KP, Bonde J, Nielsen JH, Horch S, Chorkendorff I. Identification of active edge sites for electrochemical H_2 evolution from MoS$_2$ nano-catalysts. Science. 2007; 317: 100-102.
11. Xiao P, Sk MA, Thia L, Ge X, Lim RJ, Wang JY, et al. Molybdenum phosphide as effecicient electrocatalysts for the hydrogen evolution reaction. Energy Environ Sci. 2014; 7: 2624-2629.
12. Chen Z, Cummins D, Reinecke BN, Clark E, Sunkara MK, Jaramillo TF. Core-shell MoO$_3$-MoS$_2$ nanowires for hydrogen evolution: a functional design for electrocatalytic materials. Nano Letters. 2011; 11: 4168-4175.
13. Fujishima A, Honda K. Electrochemical photolysis of water at a semiconductor electrode. Nature. 1972; 238: 37-38.

14. Li L, Yan J, Wang T, Zhao ZJ, Zhang J, Gong J, et al. Sub-10nm rutile titanium dioxide nanoparticles for efficient visible-light-driven photocatalytic hydrogen production. Nat Commun. 2015; 6: 5881.
15. Cai F, Tang Y, Shen H, Wang C, Ren A, Xiao L, et al. Graphene oxide-assisted syntehsis and photocatalytic hydrogen production of mix-phase titanium dioxide (TiO_2) nanosheets. Cryst Eng Comm. 2015; 17: 1086-1091.
16. Karnahl M, Mejía E, Rockstroh N, Tschierlei S, Luo SP, Grabown K, et al. Photocatalytic hydrogen production with copper photosensitized-titanium dioxide composites. Chem Cat Chem. 2014; 6: 82-86.
17. Liu X, Liu Z, Lu J, Wu X, Chu W. Silver sulfide nanoparticles sensitized titanium dioxide nanotube arrays syntehsized by in situ sulfurization for photocatalytic hydrogen production. J Colloid Interface Sci. 2014; 413: 17-23.
18. Yan Z, Wu H, Han A, Yu X, Du P. Noble-metal-free cobalt oxide (CoO_x) nanoparticles loaded on titanium dioxide/cadmium sulfide composite for enhanced photocatalytic hydrogen production from water. Int J Hydrog Energy. 2014; 39: 13353-13360.
19. Yan Z, Yu X, Zhang Y, Jia H, Sun Z, Du P. Enhanced visible light-driven hydrogen production from water by a noble-metal-free system containing organic dye-sensitized titanium dioxide loaded with nickel hydroxide as the cocatalyst. Appl Catal B Environ. 2014; 160: 173-178.
20. Hu MZ, Lai P, Bhuiyan MS, Tsouris C, Gu B, Paranthaman MP, et al. Synthesis and characterization of anodized titanium-oxide nanotube arrays. J Mater Sci. 2009; 44: 2820-2827.
21. Sun L, Li J, Wang C, Li S, Chen H, Lin C. An electrochemical strategy for dopping Fe^{3+} into TiO_2 nanotube array films for enhancement in photocatalytic activity. Sol Energy Mater Sol Cells. 2009; 93: 1875-1880.
22. Xie Y, Heo SH, Kim YN, Yoo SH, Cho SO. Synthesis and visible-light-induced catalytic activity of Ag_2S-coupled TiO_2 nanoparticles and nanowires. Nanotechnology. 2010; 21: 015703.
23. Nagasuna K, Akita T, Fujishima M, Tada H. Photodeposition of A_g2S quantum dots and application to photoelectrochemical cells for hydrogen production under simulated sunlight. Langmuir. 2011; 27: 7294-7300.
24. Doong RA, Hsieh TC, Huang CP. Photoassited reduction of metal ions and organic dye by titanium dioxide nanoparticles in aqueous solution under anoxic conditions. Sci Total Environ. 2010; 408: 3334-3341.
25. Xie K, Sun L, Wang C, Lai Y, Wang M, Chen H, et al. Photoelectrocatalytic properties of Ag nanoparticles loaded TiO_2 nanotube arrays prepared by pulse current deposition. Electrochim Acta. 2010; 55: 7211-7218.
26. Feng X, Sloppy JD, LaTempa TJ, Paulose M, Komarneni S, Bao N, et al. Synthesis and deposition of ultrafine Pt nanoparticles within high aspect ratio TiO_2 nanotube arrays: Application to the photoelectrocatlytic reduction of carbon dioxide. J Mater Chem. 2011; 21: 13429-13433.
27. Yin Y, Jin Z, Hou F. Enhanced solar water-splitting efficiency using core/sheath heterostructure CdS/TiO_2 nanotube arrays. Nanotechnology. 2007; 18: 495608.
28. Yang C, Wang Z, Lin T, Yin H, Lü X, Wan D, et al. Core-shell nanostructures "black" rutile titania as excellent catalyst for hydrogen production enhanced by sulfur dopping. J Am Chem Soc. 2013; 135: 17831-17838.

29. Huang L, Wang X, Yang J, Liu G, Han J, Li C. Dual cocatalysts loaded type I CdS/ZnS core/shell nanocrystals as effective and stable photocatalysts for H_2 evolution. J Phys Chem C. 2013; 117: 11584-11591.
30. Kim HS, Kim D, Kwak BS, Han GB, Um MH, Kang M. Synthesis of magnetically separable core@shell structured $NiFe_2O_4$@TiO_2 nanomaterial and its use for photocatalytic hydrogen production by methanol/water splitting. Chem Eng J. 2014; 243: 272-279.
31. Xu Z, Yin M, Sun J, Ding G, Lu L, Chang P, et al. 3D periodic multiscale TiO_2 architecture: A platform decorated with graphene quantum dots for enhanced photoelectrochemical water splitting. Nanotechnology. 2016; 27: 115401.
32. Li H, Yu H, Sun L, Zhai J, Han X. A self-assembled 3D Pt/TiO_2 architecture for high-performance photocatalytic hydrogen production. Nanoscale. 2015; 7: 1610-1615.
33. Zhang Y, Bilan HK, Podlaha E. Enhancing the hydrogen evolution reaction with Ni-W-TiO_2 composites. Electrochem Commun. 2018; 96: 108-112.
34. Wang C, Bilan HK, Podlaha EJ. Electrodeposited Co-Mo-TiO_2 electrocatalyts for hydrogen evolution reaciton. J Electrochem Soc. 2019; 166: F661-F669.
35. Parra-Cabrera C, Achille C, Kuhn S, Amellot R. 3D printing in chemical engineering and catalytic technology: Structured catalysts, mixers and reactors. Chem Soc Rev. 2018; 47: 209-230.
36. Bi Z, Paranthaman MP, Menchhofer PA, Dehoff RR, Bridges CA, Chi M, et al. Self-organized amorphous TiO_2 nanotube arrays on porous Ti foam for rechargeable lithium and sodium ion batteries. J Power Sources. 2013; 222: 461-466.
37. Heinl P, Körner C, Singer RF. Selective electron beam melting of cellular titanium: Mechanical properties. Adv Eng Mater. 2008; 10: 882-888.
38. Li X, Close T, Pustulka S, Pedu S, Xue Y, Richter C, et al. Electrosorption of monovalent alkaline metal ions onto highly-order mesoporous titanium dioxide nanotube electrodes. Electrochim Acta. 2017; 231: 632-640.
39. Li X, Pustullka S, Pedu S, Close T, Xue Y, Richter C, et al. Titanium dioxide nanotubes as model systems for electrosorption studies. Nanomaterials. 2018; 8: 404-417.
40. Richter C, Panaitescu E, Willey R, Menon L. Titania nanotubes prepared by anodization in fluorine-free acids. J Mater Res. 2007; 22: 1624-1631.
41. Richter C, Schmuttenmaer CA. Exciton-like trap states limit electron mobility in TiO_2 nanotubes. Nat Nanotechnol. 2010; 5: 769-772.
42. Conway B, Tilak B. Interfacial processes involving electrocatalytic evolution and oxidation of H_2, and the role of chemisorbed H. Electrochim Acta. 2002; 47: 3571-3594.
43. Tan Y, Wang H, Liu P, Cheng C, Zhu F, Hirata A, et al. 3D nanoporous metal phosphides toward high-efficiency electrochemical hydrogen production. Adv Mater. 2016; 28: 2951.
44. Gao MR, Chan MK, Sun Y. Edge-terminated molybdenum disulfide with a 9.4-Å interlayer spacing for electrochemical hydrogen production. Nat Commun. 2015; 6: 7493.
45. Benck JD, Chen Z, Kuritzky LY, Forman AJ, Jaramillo TF. Amorphous molybdenum sulfide catalysts for electrochemical hydrogen production: Insights into the origin of their catalytic activity. ACS Catalysis. 2012; 2: 1916-1923.
46. Ma FX, Wu HB, Xia BY, Xu CY, Lou XWD. Hierarchical b-Mo_2C nanotubes organized by ultrathin nanosheets as a highly efficient electrocatalysts for hydrogen production. Angew Chem Int Ed. 2015; 54: 15395-15399.

47. Hod I, Deria P, Bury W, Mondloch JE, Kung CW, So M, et al. A porous proton-relaying metal-organic framework material that accelerates electrochemical hydrogen evolution. Nat Commun. 2015; 6: 8304.
48. Thomas J. Kinetics of electrolytic hydrogen evolution and the adsorption of hydrogen by metals. J Chem Soc Faraday Trans. 1961; 57: 1603-1611.
49. Fletcher S. Tafel slopes from first principles. J Solid State Electr. 2009; 13: 537-549.
50. Diebold U. The surface sicence of titanium dioxide. Surf Sci Rep. 2003; 48: 53-229.
51. Thomas N, Nobe K. Kinetics of the hydrogen evolution reaction on titanium. J Electrochem Soc. 1970; 117: 622-626.
52. Shinagawa T, Garcia-Esparza AT, Takanabe K. Insight on Tafel slopes from a microkinetic analysis of aqueous electrocatalysis for energy conversion. Sci Rep. 2015; 5: 13801.